Sequential Evolution of Different Phases in Metastable Gd2-xCexZr2-xAlxO7 (0.0 <= x <= 2.0) System: Crucial Role of Reaction Conditions

ARTICLE *in* INORGANIC CHEMISTRY · JUNE 2013

Impact Factor: 4.76 · DOI: 10.1021/ic401041e · Source: PubMed

5 AUTHORS, INCLUDING:

Rakesh Shukla

University of Cincinnati

300 PUBLICATIONS **6,246** CITATIONS

SEE PROFILE

Farheen N Sayed

Rice University

23 PUBLICATIONS **170** CITATIONS

SEE PROFILE

Suhas Phapale

Bhabha Atomic Research Centre

18 PUBLICATIONS **40** CITATIONS

SEE PROFILE

Inorganic Chemistry

Article

pubs.acs.org/IC

Sequential Evolution of Different Phases in Metastable $Gd_{2-x}Ce_xZr_{2-x}Al_xO_7$ ($0.0 \leq x \leq 2.0$) System: Crucial Role of Reaction Conditions

Rakesh Shukla, Farheen N. Sayed, Suhas Phapale, Ratikant Mishra, and Avesh K. Tyagi*

Chemistry Division, Bhabha Atomic Research Centre, Mumbai 400085, India

Supporting Information

ABSTRACT: The $Gd_{2-x}Ce_xZr_{2-x}Al_xO_7$ ($0.0 \leq x \leq 2.0$) series was synthesized by the gel combustion method. This system exhibited the presence of a fluorite-type phase, along with a narrow biphasic region, depending upon the Ce/Gd content in the sample. Thermal stability of these new compounds under oxidizing and reducing conditions has been investigated. The products obtained on decomposition of $Gd_{2-x}Ce_xZr_{2-x}Al_xO_7$ in oxidizing and reducing conditions were found to be entirely different. It was observed that in air the fluorite-type solid solutions of $Gd_{2-x}Ce_xZr_{2-x}Al_xO_7$ composition undergo phase separation into perovskite $GdAlO_3$ and fluorite-type solid solutions of Gd−Ce−Zr−O or Ce−Zr−Al−O depending upon the extent of Ce and Al substitution. On the other hand, $Gd_{2-x}Ce_xZr_{2-x}Al_xO_7$ samples on heating under reducing conditions show a phase separation to $CeAlO_3$ perovskite and a defect-fluorite of $Gd_2Zr_2O_7$. The extent of metastability for a typical composition of $Gd_{1.2}Ce_{0.8}Zr_{1.2}Al_{0.8}O_7$ (nano), $Gd_{1.2}Ce_{0.8}Zr_{1.2}Al_{0.8}O_{6.6}$ (heated under reduced conditions), $Gd_{1.2}Ce_{0.8}Zr_{1.2}Al_{0.8}O_7$ (heated in air at 1200 °C) has been experimentally determined employing a high temperature Calvet calorimeter. On the basis of thermodynamic stability data, it could be inferred that the formation of a more stable compound in the presence of two competing cations (i.e., Gd^{3+} and Ce^{3+}) is guided by the crystallographic stability.

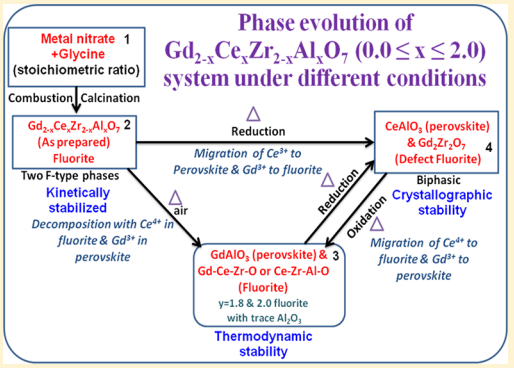

INTRODUCTION

The thermodynamic stability of any compound is primarily responsible for the formation of its most stable product, whereas, additional kinetic and crystallographic stability data provide information on local thermodynamic minima, leading to interesting metastable compounds. These metastable compounds can be isolated under appropriate conditions, if information on thermodynamic stability of the compounds is known. Among all structures, pyrochlores are considered among the most rugged matrixes that possess excellent crystal chemical flexibility.[1] In this context the phase relation studies in pyrochlore and perovskite systems are of great interest to material scientists as they help to understand the stability of the compounds as a function of temperature and composition. Phase relation study also provides information on the formation of stable compounds with respect to composition at the macroscopic level. $Gd_2Zr_2O_7$ is one of the borderline compounds that shows both pyrochlore and defect fluorite structure.[2] In $Gd_2Zr_2O_7$ compound Ce^{4+} has a limited solubility at the Zr-site.[3] In our earlier work, Ce^{3+} was substituted at the Gd^{3+} site of the $Gd_2Zr_2O_7$ pyrochlore, and the detailed phase relation in this system was studied under reducing and oxidizing conditions.[4] It was found that cerium in both 3+ and 4+ oxidation states at the A-site forms a complete range of metastable solid solution with pyrochlore structure and metastable anion-rich pyrochlore structure, respectively. In the present work, it was envisaged to obtain a range of solid solution with higher Ce^{4+}solubility in the $Gd_2Zr_2O_7$ pyrochlore structure by cosubstitution of equal amount of Al^{3+} at the Zr-site, so as to ensure that the anionic lattice of $Gd_{2-x}Ce(IV)_xZr_{2-x}Al_xO_7$ is not disturbed. It was also envisaged to stabilize a new series of Ce^{3+} anion-deficient pyrochlore ($Gd_{2-x}Ce(III)_xZr_{2-x}Al_xO_{7-x/2}$) lattices by reduction of these compounds. Thus, a complete study on phase relations of this compound by substituting the A-site by Ce^{3+}/ Ce^{4+} and the B-site by Al^{3+} ion was undertaken. The observations of the $Gd_{2-x}Ce_xZr_{2-x}Al_xO_7$ ($0.0 \leq x \leq 2.0$) phase relation under different conditions are described in the subsequent sections. It should be noted that there are no phase-equilibria studies reported on this multicomponent system, to the best of our knowledge.

EXPERIMENTAL SECTION

AR grade powders of Gd_2O_3, $ZrO(NO_3)_2{\cdot}5H_2O$, $Ce(NO_3)_3{\cdot}6H_2O$, $Al(NO_3)_3{\cdot}9H_2O$, and glycine were used as the starting reactants. $Gd_{2-x}Ce_xZr_{2-x}Al_xO_7$ ($0.0 \leq x \leq 2.0$) compositions were prepared by taking appropriate amounts of metal nitrates with glycine as a fuel in stoichiometric ratio. The gel obtained from these solutions on dehydrating was further autoignited to produce voluminous powders.

Received: January 17, 2013
Published: June 21, 2013

   dx.doi.org/10.1021/ic401041e | Inorg. Chem. 2013, 52, 7873−7880

To get rid of the decomposition products and excess carbon, the powders obtained after autoignition were calcined at 600 °C for 2 h. To reduce Ce^{4+} to Ce^{3+} in these compositions, the powders were pelletized, wrapped in tantalum foil, introduced in a quartz tube in the presence of zirconium sponge, and then vacuum sealed online (10^{-6} mbar). Zirconium sponge acts as oxygen-getter. The tube was heated at 1050 °C for 24 h. X-ray diffraction (XRD) has been recorded on all the powders using monochromatized Cu−Kα radiation on a PANalytical Xpert Pro. The standard molar enthalpies of formation of different forms of the compound, that is, $Gd_{1.2}Ce_{0.8}Zr_{1.2}Al_{0.8}O_7$ (nano), $Gd_{1.2}Ce_{0.8}Zr_{1.2}Al_{0.8}O_{6.6}$ (heated under reduced conditions), $Gd_{1.2}Ce_{0.8}Zr_{1.2}Al_{0.8}O_7$ (heated in air at 1200 °C) were determined by measuring the enthalpy of dissolution of different aforementioned forms of $Gd_{1.2}Ce_{0.8}Zr_{1.2}Al_{0.8}O_7$ compound and its corresponding constituent oxides such as Gd_2O_3(s), CeO_2(s), ZrO_2(s), and Al_2O_3(s) in liquid Na_2O + MoO_3 solvent (3:4 molar ratio) at 713 °C employing a high temperature Calvet calorimeter (Setaram, Model HT-1000). The calorimeter has an isothermal alumina block which contains two identical one-end closed alumina cells surrounded by a series of thermopiles. The temperature of the isothermal block was measured using a Pt−Pt 10% Rh thermocouple (±0.1 °C). The details of the experimental measurements have been described elsewhere.[5] The heat calibration was carried out using a synthetic sapphire [NIST SRM-720].

The solvent Na_2O and MoO_3 (3:4 molar mixture) was initially prepared by heating a mixture of perfectly dried Na_2CO_3 (BDH, reagent grade) and MoO_3 (BDH, reagent grade) in appropriate molar ratio and slowly heated in a platinum disk inside the furnace up to 713 °C. Na_2CO_3 decomposes to Na_2O forming a eutectic mixture. The melt was maintained at 713 °C for 6 h for homogenization. The mass loss of the product was monitored to ensure the correct stoichiometry of the melt. The entire substance was removed from the platinum disk by slowly scratching the melt and grinding it again to make a uniform powder. The solvent powder was characterized by chemical analysis and XRD techniques. The atom % of Mo, Na, and O obtained from the chemical analysis of the solvent were found to be 16.2 ± 0.2, 23.4 ± 0.3, and 60.4 ± 0.4, respectively. No other chemical impurity could be detected. Powder from the same lot was used in all reaction enthalpy measurements.

About 3 g of Na_2O + MoO_3 (3:4 molar) solvent was taken in each of the two identical platinum tubes which act as a protective lining and having outer diameter (OD) matching exactly with the alumina reaction cell for proper thermal contact. The reaction cell assembly was slowly lowered into the calorimeter, and the calorimeter was programmed up to 713 °C at a heating rate of 0.5 °C/min and maintained at 713 ± 0.05 °C during the whole experiment. The reaction tubes were equilibrated inside the chamber for sufficiently long time till a steady baseline for heat flux signal was achieved. The slope of the baseline of the differential heat flow signal was nearly zero since the heat effect due to any small loss of the volatile components will get nullified as the same effect was present in the sample and reference cells. Small pellets containing a few milligrams of the samples were dropped from room temperature to the reaction cell containing liquid solvent maintained at 713 °C, and the corresponding enthalpy change was determined by integrating the heat flow signal with respect to time. The time required for the completion of the reaction was determined by recording the heat flow signal (J/g) for different time intervals. The reaction time was established when a steady baseline was achieved, and the values of reaction enthalpy obtained as a function of time converged into a constant value. For each dissolution experiment the reaction time was determined, and the heat flow signals were recorded for the same time period for all experiments. Similarly, for each experiment fresh solvent was used so that the similar dilution condition was maintained. The amount of the reactant dropped into solvent was chosen in such a manner that the concentration of Gd, Ce, Zr, and Al remained well below 1 atom %. The infinite dilution condition was established by repeating the dissolution experiments on a same lot of the solvent. The consistency in the values of the reaction per unit mass of the reactants is indicative of the fact that the infinite dilution condition was maintained during the measurements.

RESULT AND DISCUSSION

The gel-combustion synthesis is a well-known method which has been successfully employed to synthesize nanocrystalline materials.[6−9] The gel-combustion process is basically a redox reaction between metal nitrate (oxidant) and a fuel like glycine, citric acid, and so forth.[9,10] The main motivation for using this preparative technique was to achieve atomistically blended constituents in the solution that reduces the possibility of side reaction, if any. Respective metal nitrates in stoichiometric amounts were dissolved in a minimum amount of distilled water. Glycine was added to the solution in 60% fuel-deficient ratio. This solution on thermal dehydration formed a gel. On further heating, the gel autoignited with large amount of gaseous evolution giving a highly porous powder. The obtained powders were calcined at 600 °C for 2 h to get rid of carbonaceous impurity, if any.

The XRD patterns of the as-prepared samples after calcination are shown in Figure 1. The nominal composition

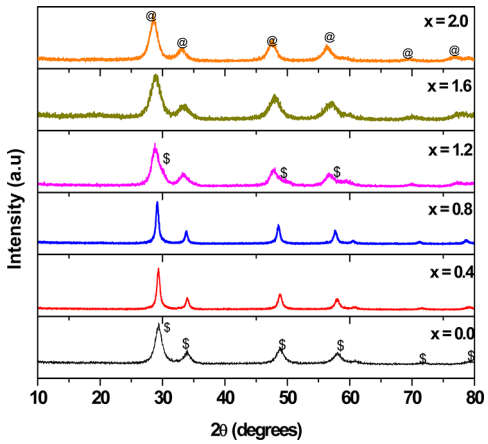

Figure 1. XRD pattern of as-prepared $Gd_{2-x}Ce_xZr_{2-x}Al_xO_7$ compositions calcined at 700 °C ($, Gd-rich phase; @, Ce-rich phase).

of the products obtained after the combustion process can be generalized as $Gd_{2-x}Ce_xZr_{2-x}Al_xO_7$ ($0.0 \le x \le 2.0$) considering the aerial oxidation of Ce^{3+} ions to Ce^{4+}.[11,12] The XRD investigation shows the presence of two single-phasic regions having fluorite-type compounds toward both the end members, with a narrow biphasic region, depending upon the x content in the samples. One of the phases can be assigned as Gd-rich fluorite-type structure with the value of x varying from 0.0 to 1.0. The other phase is Ce-rich fluorite-type structure with x varying from 1.6 to 2.0. From the asymmetry in the shape of the XRD peaks it was observed that the compositions with value of x = 1.2 (Figure 1) and 1.4 (not shown in Figure 1) show the presence of both the fluorite structures. Even though the samples were prepared under identical conditions, the FWHM of the peak was found to decrease initially in the composition with x = 0.2−1.0 and then increase from the value of x = 1.2−2.0. Initial decrease in FWHM can be attributed to the nature of the sample. On the other hand, increase in the fwhm from x = 1.2−2.0 can be attributed to the strain due to incorporation of the substituted cations in the lattice. Similar observation of increased FWHM as a function of aliovalent ion substitution was reported for the $Ce_{1-x}Nd_xO_{2-x/2}$ system in which all the samples were prepared under identical condition.[13]The variation in cell parameter as a function of substitution is shown in Figure 2. The well-defined trend of

dx.doi.org/10.1021/ic401041e | Inorg. Chem. 2013, 52, 7873−7880

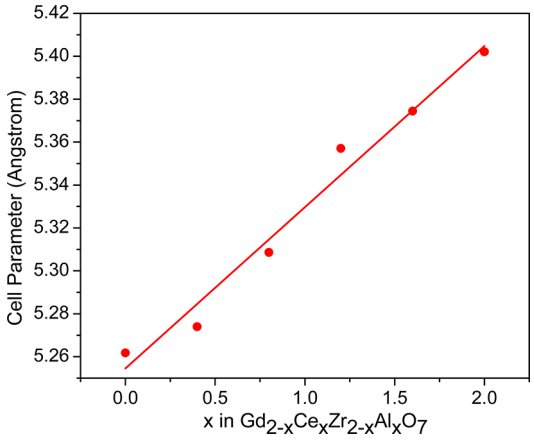

Figure 2. Cell parameter variation as function of x in $Gd_{2-x}Ce_xZr_{2-x}Al_xO_7$ calcined at 700 °C.

increase in the cell parameter is evidence of fluorite-type solid solution phase formation in the sample in the range of composition (x = 0.0–2.0). The marginal but discernible increase in the cell dimension can be attributed to the enhanced surface energy due to the increasingly nanonature of the samples. The compounds obtained after calcination were then heated at 1200 °C in air to obtain a well crystalline phase. The XRD pattern of series of compounds sintered at 1200 °C in air are shown in Figure 3. It was seen that the fluorite-type solid

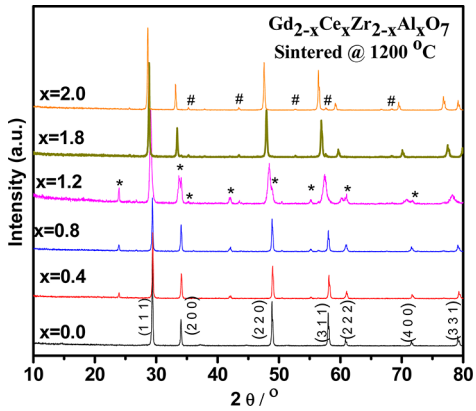

Figure 3. XRD patterns of $Gd_{2-x}Ce_xZr_{2-x}Al_xO_7$ sintered at 1200 °C in air (*, $GdAlO_3$ phase; #, Al_2O_3 and unmarked peaks are due to fluorite type phase for composition see Table 1).

solutions $Gd_{2-x}Ce_xZr_{2-x}Al_xO_7$ undergo a phase separation to $GdAlO_3$ and another fluorite-type solid solution Gd–Ce–Zr–O or Ce–Zr–Al–O depending upon the x value. The hyphenated systems (like Gd–Ce–Zr–O or Ce–Zr–Al–O) used in this manuscript hereafter will denote the fluorite-type structure whose composition depends upon the x content in the sample. Detail phase analysis of the composition is shown in Table 1(a). The XRD pattern of $GdAlO_3$ matched well with standard PCPDF card No: 46-0395. A typical Rietveld fitted pattern for $Gd_{1.0}Ce_{1.0}Zr_{1.0}Al_{1.0}O_7$ showing orthorhombic $GdAlO_3$ and fluorite-type $CeZrO_4$ phase is shown in Supporting Information, Figure S-1. The typical Rietveld fitted parameters are shown in Supporting Information, Table S-I. It can be seen that at higher temperature in air there are two to three thermodynamically stable phases, that is, perovskite $GdAlO_3$, fluorite-type structure of Gd–Ce–Zr–O or Ce–Zr–Al–O. The compositions with higher content of cerium ($x \geq 1.2$) showed the presence of weak peaks due to corundum-type Al_2O_3 also. Interestingly, still higher cerium ($x \geq 1.8$) containing samples were found to form fluorite-type structure of Gd–Ce–Zr–Al–O with slight Al_2O_3 impurity, after heating at 1200 °C in air. Thus it can be inferred that the Gd in the compositions with higher cerium content has a greater preference for dissolution to the fluorite structure over the formation of perovskite $GdAlO_3$.

Formation of fluorite solid solution over the entire range in the as-prepared sample assumes further significance, in view of the fact that at higher temperature there is limited solubility of the Al^{3+} in pyrochlore lattice or fluorite lattice, as inferred by XRD data of 1200 °C heated samples. The stability of the fluorite structure in the as-prepared sample is due to kinetic stabilization attributed to the nonequilibrium method employed and the nanocrystalline nature of the compound. Thus it can be inferred that by employing a nonequilibrium method and making the sample in the nanoregime it is possible to extend solubility leading to metastable solid solutions, which are otherwise not possible to be synthesized.[8,9] The decomposition of the metastable fluorite-type samples to perovskite and other fluorite-type phases, on heating at 1200 °C, can be explained by invoking the tolerance factor concept. Goldschmidt's tolerance factor (t) has been widely accepted as a criterion for the formation of the perovskite structure. This factor is used by many researchers for describing the stability of oxide perovskite.[14–18] The tolerance factor of $GdAlO_3$ is 0.9714 which is very close to the ideal value of 1, which makes its existence under the prevailing conditions favorable. Hence Gd

Table 1. Phase and Composition of Compounds in $Gd_{2-x}Ce_xZr_{2-x}Al_xO_7$ Series under Different Conditions

	as prepared	after reduction		after oxidaton at 1200 °C		
x in sample	Phase	Phase-I	Phase-II	Phase-I	Phase-II	Phase-III
0.0	$Gd_2Zr_2O_7$	$Gd_2Zr_2O_7$		$Gd_2Zr_2O_7$		
0.2	$Gd_{1.8}Ce_{0.2}Zr_{1.8}Al_{0.2}O_7$	0.9 $Gd_2Zr_2O_7$	0.2 $CeAlO_3$	0.2 $GdAlO_3$	$Gd_{1.6}Ce_{0.2}Zr_{1.8}O_{6.4}$	
0.4	$Gd_{1.6}Ce_{0.4}Zr_{1.6}Al_{0.4}O_7$	0.8 $Gd_2Zr_2O_7$	0.4 $CeAlO_3$	0.4 $GdAlO_3$	$Gd_{1.2}Ce_{0.4}Zr_{1.6}O_{5.8}$	
0.6	$Gd_{1.4}Ce_{0.6}Zr_{1.8}Al_{0.6}O_7$	0.7 $Gd_2Zr_2O_7$	0.6 $CeAlO_3$	0.6 $GdAlO_3$	$Gd_{0.8}Ce_{0.6}Zr_{1.4}O_{5.2}$	
0.8	$Gd_{1.2}Ce_{0.8}Zr_{1.8}Al_{0.8}O_7$	0.6 $Gd_2Zr_2O_7$	0.8 $CeAlO_3$	0.8 $GdAlO_3$	$Gd_{0.4}Ce_{0.8}Zr_{1.2}O_{4.6}$	
1.0	$Gd_{1.0}Ce_{1.0}Zr_{1.0}Al_{1.0}O_7$	0.5 $Gd_2Zr_2O_7$	$CeAlO_3$	$GdAlO_3$	2 $Ce_{0.5}Zr_{0.5}O_2$	
1.2	$Gd_{0.8}Ce_{1.2}Zr_{0.8}Al_{1.2}O_7$	0.4 $Gd_2Zr_2O_7$	1.2 $CeAlO_3$	0.8 $GdAlO_3$	$Ce_{1.2}Zr_{0.8}Al_mO_{4+1.5m}$	$(0.4 - m)/2$ Al_2O_3
1.4	$Gd_{0.6}Ce_{1.4}Zr_{0.6}Al_{1.4}O_7$	0.3 $Gd_2Zr_2O_7$	1.4 $CeAlO_3$	0.6 $GdAlO_3$	$Ce_{1.4}Zr_{0.6}Al_nO_{4+1.5n}$	$(0.4 - n)/2$ Al_2O_3
1.6	$Gd_{0.4}Ce_{1.6}Zr_{0.4}Al_{1.6}O_7$	0.2 $Gd_2Zr_2O_7$	1.6 $CeAlO_3$	0.4 $GdAlO_3$	$Ce_{1.6}Zr_{0.4}Al_pO_{4+1.5p}$	$(0.4 - p)/2$ Al_2O_3
1.8	$Gd_{0.2}Ce_{1.8}Zr_{0.2}Al_{1.8}O_7$	0.1$Gd_2Zr_2O_7$	1.8 $CeAlO_3$		$Gd_{0.2}Ce_{1.8}Zr_{0.2}Al_{0.2+q}O_{4+1.5q}$	$(0.4 - q)/2$ Al_2O_3
2.0	$Ce_2Al_2O_7$		2 $CeAlO_3$		$Ce_2Al_rO_{4+1.5r}$	$(2 - r)/2$ Al_2O_3

dx.doi.org/10.1021/ic401041e | Inorg. Chem. 2013, 52, 7873–7880

diffuses out from the nanocrystalline fluorite-type $Gd_{2-x}Ce_xZr_{2-x}Al_xO_7$ and preferentially reacts with Al^{3+} to form $GdAlO_3$. On the other hand, Ce^{4+}(0.97 Å) dissolves in $Gd_2Zr_2O_7$ forming a fluorite-type structure. The formation of fluorite structure instead of pyrochlore can be explained by the effective decrease in the average A-site radius because of incorporation of Ce^{4+} ion (r_A/r_B decreases which favors the formation of fluorite-type phase).

To observe the stability of $Gd_{2-x}Ce_xZr_{2-x}Al_xO_7$ samples under reducing conditions, the following experiments were performed. The calcined powders were ground, pelletized, and wrapped in tantalum foil and placed in quartz tube containing thin pelletized zirconium metal powder. Quartz tube was then vacuum sealed at 10^{-6} mbar pressure and heated to 1050 °C for 24 h.[19,20] During this heat treatment in the presence of Zr powder, there is a further reduction of partial pressure of O_2, which facilitates the reduction of Ce^{4+} to Ce^{3+} in the calcined fluorite $Gd_{2-x}Ce_xZr_{2-x}Al_xO_7$ compound. It was envisaged that when Ce^{4+} reduces to Ce^{3+} the average A-site radius will increase which may lead to the formation of single phasic anion-deficient pyrochlore $Gd_{2-x}Ce_xZr_{2-x}Al_xO_{7-x/2}$ compositions. From the ASTD[21] data it was found that the oxygen partial pressure required to obtain Ce^{3+} (Ce_2O_3) from Ce^{4+} (CeO_2) at 1050 °C is 4×10^{-18} atmospheric pressure. The sample was wrapped in a tantalum foil and enclosed in an evacuated quartz tube with internal volume 25 cm^3 and 10^{-6} mbar pressure. The sample was heated at 1050 °C for 24 h assuming that the rate of diffusion of oxygen through the quartz tube is negligible. The volume ratio between the Zr pellets and the internal volume is approximately 0.25. Under this condition an equilibrium reaction between Zr and ZrO_2 will be established. The equilibrium partial pressure of oxygen under this condition as calculated using standard thermodynamic data[21] is found to be 2.7×10^{-34} atmosphere. Since at the end of experiment we observed the coexistence of Zr metal and negligibly small amount of ZrO_2, it was inferred that the equilibrium prevailed with partial pressure of oxygen as 2.7×10^{-34} atmosphere at 1050 °C. The calculated partial pressure is considerably lower than the pressure required to obtain Ce^{3+} (Ce_2O_3) from Ce^{4+} (CeO_2) and hence Ce^{3+} was stabilized during the reaction.

The XRD pattern of the reduced series of sample is shown in Figure 4. A typical Rietveld fitted pattern for $Gd_{1.0}Ce_{1.0}Zr_{1.0}Al_{1.0}O_7$ showing tetragonal $CeAlO_3$ and defect fluorite $Gd_2Zr_2O_7$ phase and single phasic tetragonal $CeAlO_3$ is shown in Supporting Information, Figures S-2 and S-3, respectively. The typical Rietveld fitted parameters are shown in Supporting Information, Table S-I. Interestingly, it was observed that instead of forming a single phasic anion-deficient pyrochlore structure, the heat treatment in the reducing conditions led to the formation of a biphasic product accompanied by swapping of Gd^{3+} and Ce^{3+} cations, as under these conditions $CeAlO_3$ (PCPDF card No: 81-1186) and $Gd_2Zr_2O_7$ (PCPDF card No: 80-0471) were formed. Formation of $CeAlO_3$ instead of $GdAlO_3$ could also be explained using the tolerance factor concept. The tolerance factor of $CeAlO_3$ is 1.003 and $GdAlO_3$ is 0.9714; thus, crystallographically $CeAlO_3$ is more favorable and in turn it is formed. Under these conditions the formation of pyrochlore $Ce_2Zr_2O_7$ is also favorable. However, the formation of $CeAlO_3$ showed that the perovskite lattice was more favorable and stable over the $Ce_2Zr_2O_7$ pyrochlore lattice.

To observe the behavior of these reduced samples under the oxidative conditions, the samples were heated in air at two different temperatures, namely, 900 and 1200 °C. The XRD patterns of the sample heated at 900 and 1200 °C are shown in Figures 5 and 6, respectively. It was seen that $CeAlO_3$ is retained up to 900 °C; however, at 1200 °C $CeAlO_3$ decomposes to give a fluorite structure (i.e., Al^{3+} substituted CeO_2) with slight Al_2O_3 impurity due to phase separation attributed to the partial immiscibility of Al^{3+} in CeO_2 lattice.

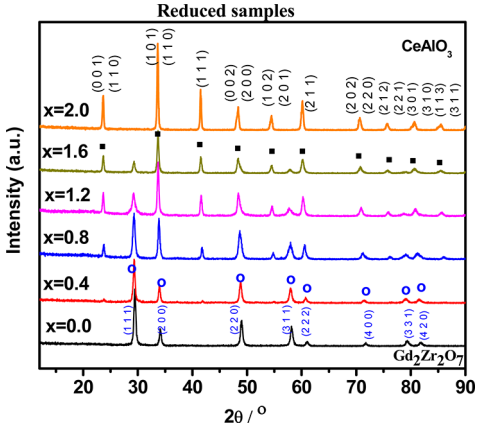

Figure 4. XRD patterns of $Gd_{2-x}Ce_xZr_{2-x}Al_xO_{7-x/2}$ after reduction in the presence of Zr sponge ■, $CeAlO_3$ phase; **o**, $Gd_2Zr_2O_7$.

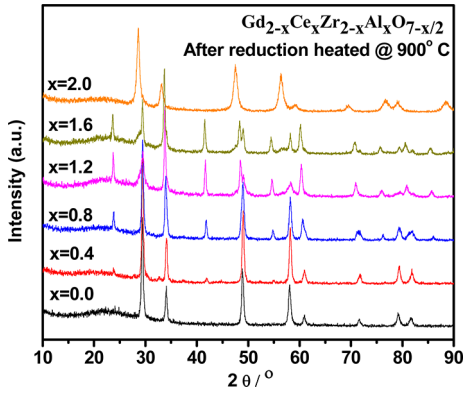

Figure 5. XRD pattern of reduced $Gd_{2-x}Ce_xZr_{2-x}Al_xO_{7-x/2}$ after heating at 900 °C in air.

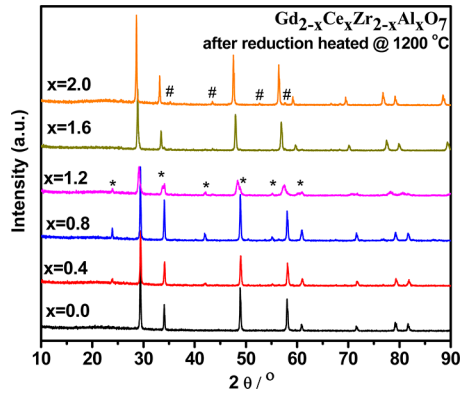

Figure 6. XRD pattern of reduced $Gd_{2-x}Ce_xZr_{2-x}Al_xO_{7-x/2}$ after heating at 1200 °C in air (*, $GdAlO_3$ phase; #, Al_2O_3; and unmarked peaks are due to fluorite type phase for composition see Table 1).

dx.doi.org/10.1021/ic401041e | Inorg. Chem. 2013, 52, 7873−7880

Under these conditions for the sample (x = 0.2 to 1.8), redistribution of cations occurs. In samples with x = 0.2 to 1.8, equal amounts of Al and Gd diffuse from $CeAlO_3$ and $Gd_2Zr_2O_7$, respectively, to form $GdAlO_3$, and the balance cations form fluorite-type Gd−Ce−Zr−O or Ce−Zr−Al−O solid solutions, depending upon the x content. The formation of perovskite solid solution with composition $Ce_{1-\delta}Gd_{\delta}AlO_3$ can be ruled out as on oxidation of Ce from 3+ to 4+ state the oxygen content in the perovskite lattice will increase, which destabilizes the perovskite lattice as it cannot accommodate the extra oxygen.

When these biphasic products, containing $GdAlO_3$ and Gd−Ce−Zr−O or Ce−Zr−Al−O fluorite solid-solutions phases, were once again reduced in the presence of Zr sponge, $CeAlO_3$ and $Gd_2Zr_2O_7$ are again obtained (XRD not shown). Thus by mere reduction and oxidation, the $GdAlO_3$ and $CeAlO_3$ compounds can be interconverted within the $Gd_{2-x}Ce_xZr_{2-x}Al_xO_7$ ($0.0 \leq x \leq 2.0$) matrix. This entire process can be summarized in the form of a flowchart as shown in Figure 7. It can be inferred that the combustion synthesis

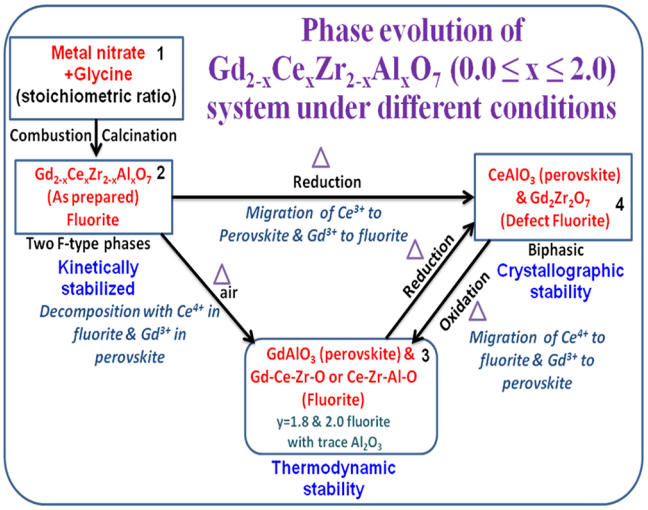

Figure 7. Phase evolution of $Gd_{2-x}Ce_xZr_{2-x}Al_xO_7$ system under different conditions.

(Block-1 of Figure 7) of the $Gd_{2-x}Ce_xZr_{2-x}Al_xO_7$ system leads to formation of two fluorite structures depending upon the Ce/Gd content in the samples. The stability of the fluorite structures is due to kinetic stabilization attributed to the nonequilibrium method employed and the nanoregime of the compound as shown in the Block-2 of Figure 7. The samples on further heating at 1200 °C in air resulted in the formation of $GdAlO_3$ and a defect fluorite solid solution of Gd−Ce−Zr−O or Ce−Zr−Al−O as shown in Block-3 of Figure 7. The compounds obtained are thus governed by the thermodynamic stability of the material under air at one atmospheric condition. On the other hand, the as-prepared samples on heating under reducing atmosphere give $CeAlO_3$ and a defect fluorite of $Gd_2Zr_2O_7$ as shown in Block-4 of Figure 7, which can be attributed to the better crystallographic stability of $CeAlO_3$ over $GdAlO_3$ structure.

To quantify the extent of metastability in the as-prepared nanosamples, typical compositions of $Gd_{1.2}Ce_{0.8}Zr_{1.2}Al_{0.8}O_7$ (nano), and corresponding $Gd_{1.2}Ce_{0.8}Zr_{1.2}Al_{0.8}O_{6.6}$ (heated under reduced conditions), $Gd_{1.2}Ce_{0.8}Zr_{1.2}Al_{0.8}O_7$ (heated in air at 1200 °C) were selected. Standard enthalpy of formation of these compounds was calculated by Calvet calorimetry. Figure 8(a−d) gives the heat flow signals for the dropping of

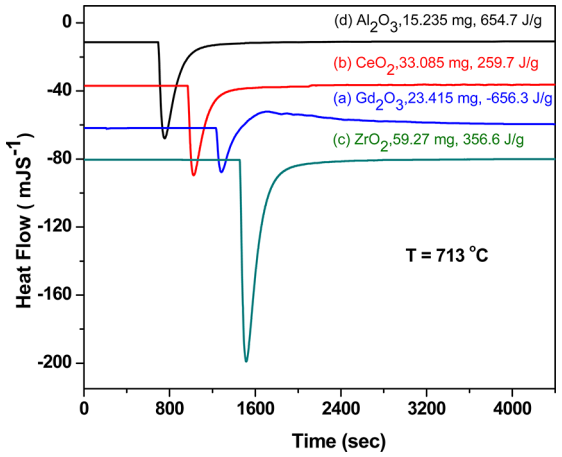

Figure 8. Heat flow signal for dropping of constituent oxides (a) Gd_2O_3, (b) CeO_2, (c) ZrO_2, and (d) Al_2O_3.

23.415, 33.085, 59.270, and 15.235 mg of Gd_2O_3(s), CeO_2(s), ZrO_2(s), and Al_2O_3(s) samples from room temperature to liquid Na_2O + MoO_3 (3:4 molar ratio) solvent maintained at 713 °C, while Figure 9(a−c) shows the heat flow signals for the

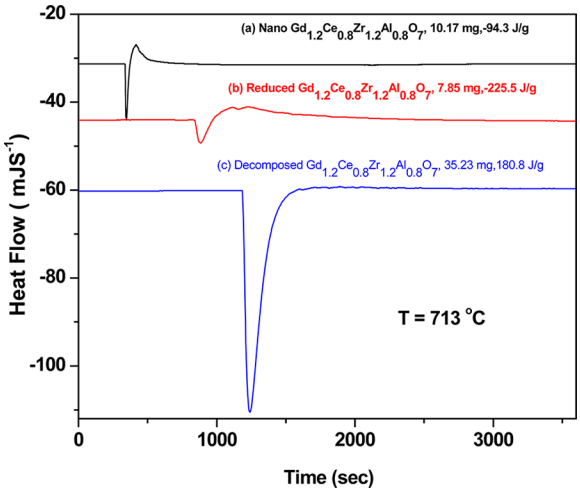

Figure 9. Heat flow signal for dropping of samples (a) nano-$Gd_{1.2}Ce_{0.8}Zr_{1.2}Al_{0.8}O_7$, (b) reduced-$Gd_{1.2}Ce_{0.8}Zr_{1.2}Al_{0.8}O_{6.6}$, (c) decomposed-$Gd_{1.2}Ce_{0.8}Zr_{1.2}Al_{0.8}O_7$.

dropping of 10.17, 7.85, and 35.23 mg $Gd_{1.2}Ce_{0.8}Zr_{1.2}Al_{0.8}O_7$ (s, nano), and corresponding $Gd_{1.2}Ce_{0.8}Zr_{1.2}Al_{0.8}O_{6.6}$ (s, heated under reduced conditions), $Gd_{1.2}Ce_{0.8}Zr_{1.2}Al_{0.8}O_7$ (s, heated in air at 1200 °C) samples. In each dropping an endothermic signal followed by a superimposed exothermic signal was observed. The completion of the reaction between the reactants and the solvent was monitored by recording the heat flow signal for different time intervals. Steady baseline in the heat flow signal was observed after 1800 s of sample dropping beyond which no significant change in the heat flow values could be noticed. Therefore a total of 1 h (3600 s) measurement time including 600 s for the baseline measurement was selected for each experiment. For comparison purpose heat flow signals are shown for 3600 s for all the measurements. The overall heat effect for dissolution in liquid

dx.doi.org/10.1021/ic401041e | Inorg. Chem. 2013, 52, 7873−7880

Table 2. Molar Enthalpies of Dissolution of Gd_2O_3(s), CeO_2(s), ZrO_2(s), Al_2O_3(s), $Gd_{1.2}Ce_{0.8}Zr_{1.2}Al_{0.8}O_7$ (s, nano), $Gd_{1.2}Ce_{0.8}Zr_{1.2}Al_{0.8}O_{6.6}$ (s, reduced), and $Gd_{1.2}Ce_{0.8}Zr_{1.2}Al_{0.8}O_7$ (s, decomposed) in 3 g of Liquid Na_2O + MoO_3 3:4 Molar Solvent at T = 713 °C[a]

compound	mass, m/mg	ΔH J g^{-1}	ΔH_T kJ mol^{-1}	$\Delta H_{increment}$ kJ mol^{-1}	$\Delta H_{dissolution}$/ kJ mol^{-1}
Gd_2O_3(s) Mol. wt. = 362.50	23.415	−656.3	−237.91	84.187	−322.10
CeO_2(s) Mol. wt. = 172.11	33.085	259.7	44.70	50.65	−5.95
ZrO_2(s) Mol. wt. = 123.22	59.27	356.6	43.94	47.93	−3.99
Al_2O_3(s) Mol. wt. = 101.96	15.235	654.7	66.75	74.55	−7.80
$Gd_{1.2}Ce_{0.8}Zr_{1.2}Al_{0.8}O_7$ (s, nano) Mol. wt. = 543.844	10.17	−94.3	−51.28	178.35	−229.63
$Gd_{1.2}Ce_{0.8}Zr_{1.2}Al_{0.8}O_{6.6}$ (s, reduced) Mol. Wt. = 537.444	7.85	−225.5	−121.19	178.354	−299.54
$Gd_{1.2}Ce_{0.8}Zr_{1.2}Al_{0.8}O_7$(s,decomp.) Mol. Wt. = 543.844	35.23	180.8	98.33	178.36	−80.03

[a] m denotes the mass of the sample dissolved; ΔH is the measured energy change per unit mass, and ΔH_T is the molar enthalpy of solution.

Table 3. Reaction Scheme for the Standard Molar Enthalpy of Formation of $Gd_{1.2}Ce_{0.8}Zr_{1.2}Al_{0.8}O_7$ (s,nano) and $Gd_{1.2}Ce_{0.8}Zr_{1.2}Al_{0.8}O_7$ (s,decomposed)[a]

reaction	ΔH_i	ΔH_i kJ mol^{-1}	reference
Nano: $Gd_{1.2}Ce_{0.8}Zr_{1.2}Al_{0.8}O_7$(s, nano, 298K) + (sln, 986 K) = 0.6Gd_2O_3(sln, 986 K) + 0.8CeO_2(sln, 986 K) + 1.2ZrO_2(sln, 986 K) + 0.4Al_2O_3(sln, 986 K)	ΔH_{nano}	−229.63	this work
Decomposed: $Gd_{1.2}Ce_{0.8}Zr_{1.2}Al_{0.8}O_7$(s, decompsed, 298 K) + (sln, 986 K) = 0.6Gd_2O_3(sln, 986 K) +0.8CeO_2(sln, 986 K) +1.2ZrO_2(sln, 986 K) + 0.4Al_2O_3(sln, 986 K)	ΔH_{decomp}	−80.03	this work
Gd_2O_3(s, 298 K) + (sln, 986 K) = Gd_2O_3(sln, 986 K)	ΔH_2	−322.10	this work
CeO_2(s, 298 K) + (sln, 986 K) = CeO_2(sln, 986 K)	ΔH_3	−5.95	this work
ZrO_2(s, 298 K) + (sln, 986 K) = ZrO_2 (sln, 986 K)	ΔH_4	−3.99	this work
Al_2O_3(s, 298 K) + (sln, 986 K) = Al_2O_3(sln, 986 K)	ΔH_5	−7.80	this work
2 2Gd(s, 298 K) + 3/2O_2(g, 298 K) = Gd_2O_3(s, 298 K)	ΔH_6	−1816.63	ref. 22
2 Ce(s, 298 K) + O_2(g, 298 K) = CeO_2(s, 298 K)	ΔH_7	−1090.40	ref. 22
2 Zr(s, 298 K) + O_2(g, 298 K) = ZrO_2(s, 298 K)	ΔH_8	−1101.29	ref. 22
2 2Al(s, 298 K) + 3/2O_2(g, 298 K) = Al_2O_3(s, 298 K)	ΔH_9	−1678.16	ref. 22
Nano: 1.2Gd(s, 298 K) + 0.8Ce(s, 298 K) + 1.2Zr(s, 298 K) + 0.8Al(s, 298 K) + 3.5O_2(g, 298 K) = $Gd_{1.2}Ce_{0.8}Zr_{1.2}Al_{0.8}O_7$(s, 298 K)	$\Delta_f H°_{298}$,nano	−3931.37	this work
Decomposed: 1.2Gd(s, 298 K) + 0.8Ce(s, 298 K) +1.2Zr(s, 298 K) +0.8Al(s, 298 K) + 3.5O_2(g, 298 K) = $CeAlO_3$(s, 298 K) + $Gd_2Zr_2O_7$(s, 298 K)	$\Delta_f H°_{298}$,decomp	−4080.98	

[a] M(sln) = dilute solution of species M in 3 g of liquid Na_2O + MoO_3 3:4 molar solvent maintained at 713 °C ($\Delta_f H°_{298\ (nano/decomposed)}$ = $-\Delta H_{nano}$/ $-\Delta H_{decomp}$ + 0.6ΔH_2 + 0.8ΔH_3 + 1.2ΔH_4 + 0.4ΔH_5 +0.6ΔH_6 + 0.8ΔH_7+1.2ΔH_8 + 0.4ΔH_9).

Na_2O + MoO_3 (3:4 molar ratio) solvent was calculated considering both endothermic and exothermic effects using the SETSOFT software supplied along with the instrument. The values of molar enthalpies of dissolution of $Gd_{1.2}Ce_{0.8}Zr_{1.2}Al_{0.8}O_7$ (nano), and corresponding $Gd_{1.2}Ce_{0.8}Zr_{1.2}Al_{0.8}O_{6.6}$ (heated under reduced conditions), $Gd_{1.2}Ce_{0.8}Zr_{1.2}Al_{0.8}O_7$ (heated in air at 1200 °C), Gd_2O_3(s), CeO_2(s), ZrO_2(s), and Al_2O_3(s) in liquid Na_2O + MoO_3 3:4 molar solvent at T = 713 °C are given in Table 2. The reaction enthalpy for each reactant with the solvent was determined by integrating the heat flow versus time signal. The average enthalpy change for dropping of $Gd_{1.2}Ce_{0.8}Zr_{1.2}Al_{0.8}O_7$ (nano), and corresponding $Gd_{1.2}Ce_{0.8}Zr_{1.2}Al_{0.8}O_{6.6}$ (heated under reduced conditions), $Gd_{1.2}Ce_{0.8}Zr_{1.2}Al_{0.8}O_7$ (heated in air at 1200 °C), Gd_2O_3(s), CeO_2, ZrO_2(s), and Al_2O_3(s) are found to be −51.28, −121.19, 98.33, −237.91, 44.70, 43.94, 66.75 kJ mol^{-1}. This enthalpy change was attributed to the sum of the endothermic heat effects due to the enthalpy increment from 25 to 713 °C and the heat effect due chemical reaction of solute with the solvent at 713 °C. The heat effect for the enthalpy increment for solute compounds was calculated from the integration of heat capacity equation, that is, $\Delta H = \int_{298}^{986} Cp_{solute}\, dT$, using reference data.[22] The values of calculated enthalpy increment for $Gd_{1.2}Ce_{0.8}Zr_{1.2}Al_{0.8}O_7$ (s, nano), $Gd_{1.2}Ce_{0.8}Zr_{1.2}Al_{0.8}O_{6.6}$ (s, reduced), $Gd_{1.2}Ce_{0.8}Zr_{1.2}Al_{0.8}O_7$ (s, air heated), Gd_2O_3(s), CeO_2, ZrO_2(s), and Al_2O_3(s) from 25 to 713 °C are also listed in Table 2. Heat capacity data for the complex oxide $Gd_{1.2}Ce_{0.8}Zr_{1.2}Al_{0.8}O_7$ (s, nano), $Gd_{1.2}Ce_{0.8}Zr_{1.2}Al_{0.8}O_{6.6}$ (s, reduced), and $Gd_{1.2}Ce_{0.8}Zr_{1.2}Al_{0.8}O_7$ (s, air heated) were calculated from heat capacity values of constituent oxide Gd_2O_3(s), CeO_2, ZrO_2(s), and Al_2O_3(s) and Ce_2O_3(s) (for reduced sample) using Neumann−Kopp rule. Subtracting the enthalpy increment value from the total measured enthalpy change, the heat effect due to dissolution of reactants was calculated. The enthalpy of dissolution ($\Delta H_{dissolution}$) of $Gd_{1.2}Ce_{0.8}Zr_{1.2}Al_{0.8}O_7$(s, nano), $Gd_{1.2}Ce_{0.8}Zr_{1.2}Al_{0.8}O_7$ (s, reduced), $Gd_{1.2}Ce_{0.8}Zr_{1.2}Al_{0.8}O_7$ (s, air heated), Gd_2O_3(s), CeO_2(s), ZrO_2(s), and Al_2O_3(s) in liquid Na_2O + MoO_3 (3:4 molar ratio) solvent at 713 °C were found to be −229.63, −299.54, −80.03, −322.10, −5.95, −3.99, and −7.80 kJ/mol, respectively. The frozen products from each calorimetric measurement dissolved in distilled water at ∼60 °C gave clear solutions indicating that the added reactants are completely dissolved in the solvent and dispersed as ions, not as compounds.

Standard Enthalpy of Formation of $Gd_{1.2}Ce_{0.8}Zr_{1.2}Al_{0.8}O_7$ (Nano) and $Gd_{1.2}Ce_{0.8}Zr_{1.2}Al_{0.8}O_7$ (Air Heated). The standard molar enthalpies of formation of

dx.doi.org/10.1021/ic401041e | Inorg. Chem. 2013, 52, 7873−7880

Table 4. Reaction Scheme for the Standard Molar Enthalpy of Formation of $Gd_{1.2}Ce_{0.8}Zr_{1.2}Al_{0.8}O_{6.6}$ (s, reduced)[a]

reaction	ΔH_i	ΔH_i kJ mol^{-1}	reference
Reduced: $Gd_{1.2}Ce_{0.8}Zr_{1.2}Al_{0.8}O_{6.6}$(s, reduced, 298 K) + (sln, 986 K) + 0.2O_2(g) = 0.6Gd_2O_3(sln, 986 K) + 0.8CeO_2(sln, 986 K) +1.2ZrO_2(sln, 986 K) + 0.4Al_2O_3(sln, 986 K)	$\Delta H_{reduced}$	−299.54	this work
Gd_2O_3(s, 298 K) + (sln, 986 K) = Gd_2O_3(sln, 986 K)	ΔH_2	−322.10	this work
CeO_2(s, 298 K) + (sln, 986 K) = CeO_2(sln, 986 K)	ΔH_3	−5.95	this work
ZrO_2(s, 298 K) + (sln, 986 K) = ZrO_2 (sln, 986 K)	ΔH_4	−3.99	this work
Al_2O_3(s, 298 K) + (sln, 986 K) = Al_2O_3(sln, 986 K)	ΔH_5	−7.80	this work
2 2Gd(s, 298 K) + 3/2O_2(g, 298 K) = Gd_2O_3(s, 298 K)	ΔH_6	−1816.63	ref. 22
2 Ce(s, 298 K) + O_2(g, 298 K) = CeO_2(s, 298 K)	ΔH_7	−1090.40	ref. 22
2 Zr(s, 298 K) + O_2(g, 298 K) = ZrO_2(s, 298 K)	ΔH_8	−1101.29	ref. 22
2 2Al(s, 298 K) + 3/2O_2(g, 298 K) = Al_2O_3(s, 298 K)	ΔH_9	−1678.16	ref. 22
Reduced 1.2Gd(s, 298 K) + 0.8Ce(s, 298 K) + 1.2Zr(s, 298 K) + 0.8Al(s, 298 K) + 3.3O_2(g, 298 K) = $Gd_{1.2}Ce_{0.8}Zr_{1.2}Al_{0.8}O_{6.6}$(s, 298 K)	$\Delta_f H^\circ_{298,\ reduced}$	−3861.44	this work

[a]M(sln) = dilute solution of species M in 3 g of liquid Na_2O + MoO_3 3:4 molar solvent maintained at 713 °C ($\Delta_f H^\circ_{298,reduced} = -\Delta H_{reduced} + 0.6\Delta H_2 + 0.8\Delta H_3 + 1.2\Delta H_4 + 0.4\Delta H_5 + 0.6\Delta H_6 + 0.8\Delta H_7 + 1.2\Delta H_8 + 0.4\Delta H_9$).

$Gd_{1.2}Ce_{0.8}Zr_{1.2}Al_{0.8}O_7$ (s, nano) and $Gd_{1.2}Ce_{0.8}Zr_{1.2}Al_{0.8}O_7$ (s, air heated) were derived using the thermochemical cycles given in Table 3. The values for molar enthalpies of dissolution ($\Delta H_{dissolution}$) of $Gd_{1.2}Ce_{0.8}Zr_{1.2}Al_{0.8}O_7$ (s, nano), $Gd_{1.2}Ce_{0.8}Zr_{1.2}Al_{0.8}O_7$ (s, air heated), Gd_2O_3(s), CeO_2(s), ZrO_2(s) and Al_2O_3(s) were combined together with other auxiliary data such as standard molar enthalpies of formation of Gd_2O_3(s), CeO_2(s), ZrO_2(s), Al_2O_3(s) from the literature[22] to derive the standard molar enthalpy of formation of $Gd_{1.2}Ce_{0.8}Zr_{1.2}Al_{0.8}O_7$(s, nano) and $Gd_{1.2}Ce_{0.8}Zr_{1.2}Al_{0.8}O_7$(s, air heated) at 25 °C. The values are found to be −3931.37 and −4080.98 kJ mol^{-1}, respectively. Thus the air heated $Gd_{1.2}Ce_{0.8}Zr_{1.2}Al_{0.8}O_7$ sample is less stable compared to as-prepared metastable $Gd_{1.2}Ce_{0.8}Zr_{1.2}Al_{0.8}O_7$ by 149.61 kJ mol^{-1}.

Standard Enthalpy of Formation of $Gd_{1.2}Ce_{0.8}Zr_{1.2}Al_{0.8}O_{6.6}$ (Reduced). $Gd_{1.2}Ce_{0.8}Zr_{1.2}Al_{0.8}O_{6.6}$ (s, reduced) compound is expected to get oxidized to net $Gd_{1.2}Ce_{0.8}Zr_{1.2}Al_{0.8}O_7$ in Na_2O + MoO_3 (3:4 molar) solvent equilibrated in static air during dissolution process. The thermo chemical cycle (Table 4) to determine the standard molar enthalpy of formation of $Gd_{1.2}Ce_{0.8}Zr_{1.2}Al_{0.8}O_7$ (s, reduced) was modified suitably to consider the reduced state of cerium ion. The values for molar enthalpies of dissolution ($\Delta H_{dissolution}$) of $Gd_{1.2}Ce_{0.8}Zr_{1.2}Al_{0.8}O_{6.6}$(s, reduced), Gd_2O_3(s), CeO_2(s), ZrO_2(s), and Al_2O_3(s) were combined together with other auxiliary data such as standard molar enthalpies of formation of Gd_2O_3(s), Ce_2O_3(s), ZrO_2(s), and Al_2O_3(s) and values of heat of oxidation of Ce_2O_3(s) at 298 K from the literature[22] to derive the standard molar enthalpy of formation of $Gd_{1.2}Ce_{0.8}Zr_{1.2}Al_{0.8}O_{6.6}$(s, reduced) at 25 °C. The value is found to be −3861.46 kJ mol^{-1}. Thus the reduced net composition $Gd_{1.2}Ce_{0.8}Zr_{1.2}Al_{0.8}O_{6.6}$ is more stable compared to as-prepared metastable $Gd_{1.2}Ce_{0.8}Zr_{1.2}Al_{0.8}O_7$ by 69.91 kJ mol^{-1}. On the basis of the above experiment it can be inferred that the most stable samples in this system are the 1200 °C air heated samples, followed by the reduced samples, and the least stable samples are the kinetically stabilized as prepared samples in nanoform.

CONCLUSION

The detailed phase relation studies have been carried out for the series $Gd_{2-x}Ce_xZr_{2-x}Al_xO_7$ under different conditions. Two types of metastable nanocrystalline fluorite-type solid solutions in the entire range have been observed. Formation of the particular fluorite-type phase is dependent on Ce/Gd content in the sample. The transformation of $Gd_{2-x}Ce_xZr_{2-x}Al_xO_7$ metastable phases to perovskite $CeAlO_3$ and defect-fluorite $Gd_2Zr_2O_7$ has been observed under the reducing conditions. At higher temperature in air, swapping of Ce^{3+} and Gd^{3+} cations occurs resulting in the formation of perovskite $GdAlO_3$ and fluorite-type Gd−Ce−Zr−O or Ce−Zr−Al−O phases. The standard molar enthalpy of formation of $Gd_{1.2}Ce_{0.8}Zr_{1.2}Al_{0.8}O_7$ (nano), $Gd_{1.2}Ce_{0.8}Zr_{1.2}Al_{0.8}O_{6.6}$ (reduced), and $Gd_{1.2}Ce_{0.8}Zr_{1.2}Al_{0.8}O_7$ (air heated) at 298 K are found to be −3931.37, − 3861.46, and −4080.98 kJ mol^{-1}, respectively. Thus it can be inferred that if there are two competing cations (Gd^{3+} and Ce^{3+}) available for the formation of a stable compound, then the compound ($GdAlO_3$ or $CeAlO_3$) thus obtained will be governed by the kinetic stability of the material under the given conditions. These observations are likely to have implication in the design of new oxygen-storage capacitors.

ASSOCIATED CONTENT

Supporting Information

Further details are given in Table S-I and Figures S-1 to S-3. This material is available free of charge via the Internet at http://pubs.acs.org.

AUTHOR INFORMATION

Corresponding Author

*E-mail: aktyagi@barc.gov.in. Phone: 0091-22-2559 5330. Fax: 0091-22-25505151

Notes

The authors declare no competing financial interest.

REFERENCES

(1) Lumpkin, G. R.; Smith, K. L.; Gieré, R.; Williams, C. T. *Geol. Soc., London, Special Pub.* **2004**, *236*, 89.

(2) Sanjay Kumar, N. R.; Chandra Shekar, N. V.; Sahu, P. Ch. *Solid State Commun.* **2008**, *147*, 357.

(3) Patwe, S. J.; Ambekar, B. R.; Tyagi, A. K. *J. Alloys Compd.* **2005**, *389*, 243.

(4) Mandal, B. P.; Shukla, R.; Achary, S. N.; Tyagi, A. K. *Inorg. Chem.* **2010**, *49*, 10415.
(5) Prasad, R.; Agarwal, R.; Roy, K.; Iyer, V.; Venugopal, V.; Sood, D. D. *J. Nucl. Mater.* **1989**, *167*, 26.
(6) Kingsley, J. J.; Suresh, K.; Patil, K. C. *J. Mater. Sci.* **1990**, *25*, 1305.
(7) Ferreira, V. M.; Azough, F.; Baptista, J. L.; Freer, R. *Ferroelectrics* **1992**, *133*, 127.
(8) Bhaduri, S.; Bhaduri, S. B.; Zhou, E. J. *J. Mater. Res.* **1998**, *13*, 156.
(9) Shukla, R.; Arya, A.; Tyagi, A. K. *Inorg. Chem.* **2010**, *49*, 1152.
(10) Purohit, R. D.; Sharma, B. P.; Pillai, K. T.; Tyagi, A. K. *Mater. Res. Bull.* **2001**, *36*, 2711.
(11) Achary, S. N.; Sali, S. K.; Kulkarni, N. K.; Krishna, P. S. R.; Shinde, A. B.; Tyagi, A. K. *Chem. Mater.* **2009**, *21*, 5848.
(12) Kishimoto, H.; Takahisa, O.; Otsuka-Yao-Matsuo, S.; Ueda, K.; Hosono, H.; Kawazoe, H. *J. Alloys Compd.* **2000**, *312*, 94.
(13) Bedekar, V.; Tyagi, A. K. *J. Nanosci. Nanotechnol.* **2007**, *7*, 3214.
(14) Liu, X.; Hong, R.; Tian, C. *J. Mater. Sci.: Mater. Electron.* **2009**, *20*, 323.
(15) Wood, E. A. *Acta Crystallogr.* **1951**, *4*, 353.
(16) Moreau, J. M. *Mater. Res. Bull.* **1968**, *3*, 427.
(17) Shannon, R. D. *Inorg. Chem.* **1967**, *6*, 1474.
(18) Babel, D. *Z. Anorg. Allg. Chem.* **1969**, *369*, 117.
(19) Shukla, R.; Bera, A. K.; Yusuf, S. M.; Deshpande, S. K.; Tyagi, A. K.; Hermes, W.; Eul, M.; Pöttgen, R. *J. Phys. Chem. C* **2009**, *113*, 12663.
(20) Shukla, R.; Manjanna, J.; Bera, A. K.; Yusuf, S. M.; Tyagi, A. K. *Inorg. Chem.* **2009**, *48*, 11691.
(21) Belov, G. V.; Trusev, B. G. *ASTD*, Computer aided Reference Book in Thermodynamical, Thermochemical &Thermophysical properties of species, Version 2.0; Moscow, 1983−1995.
(22) Kubaschewski, O.; Alcock, C. B. and Spencer, P. J. *Materials Thermochemistry*, 6th ed.; Pergamon Press,: Oxford, U.K., 1993.